Organic Covalent Patterning of Nanostructured Graphene with Selectivity at the Atomic Level

Juan Jesús Navarro,[†] Sofía Leret,[†] Fabián Calleja,[†] Daniele Stradi,[†,‡] Andrés Black,[†,§] Ramón Bernardo-Gavito,[†,§] Manuela Garnica,[†,§] Daniel Granados,[†] Amadeo L. Vázquez de Parga,*[,†,§] Emilio M. Pérez,*[,†] and Rodolfo Miranda[†,§]

[†]IMDEA Nanociencia, Calle Faraday 9, Cantoblanco 28049, Madrid, Spain
[‡]Departamento de Química, Módulo 13 and [§]Departamento de Física de la Materia Condensada and IFIMAC, Universidad Autónoma de Madrid, Cantoblanco 28049, Madrid, Spain

S *Supporting Information*

ABSTRACT: Organic covalent functionalization of graphene with long-range periodicity is highly desirable—it is anticipated to provide control over its electronic, optical, or magnetic properties—and remarkably challenging. In this work we describe a method for the covalent modification of graphene

with strict spatial periodicity at the nanometer scale. The periodic landscape is provided by a single monolayer of graphene grown on Ru(0001) that presents a moiré pattern due to the mismatch between the carbon and ruthenium hexagonal lattices. The moiré contains periodically arranged areas where the graphene−ruthenium interaction is enhanced and shows higher chemical reactivity. This phenomenon is demonstrated by the attachment of cyanomethyl radicals ($CH_2CN^\bullet$) produced by homolytic breaking of acetonitrile (CH_3CN), which is shown to present a nearly complete selectivity (>98%) binding covalently to graphene on specific atomic sites. This method can be extended to other organic nitriles, paving the way for the attachment of functional molecules.

KEYWORDS: *Nanostructured graphene, epitaxial graphene, chemical functionalization, scanning tunneling microscopy*
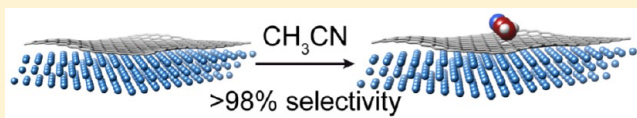
Graphene is a bidimensional network of sp^2-hybridized carbon atoms. The planar hexagonal arrangement of carbon in graphene, its chemical stability, and most significantly, its extraordinary physical properties all stem from the extended conjugation provided by the homogeneous sp^2 hybridization.[1] The chemical functionalization of graphene has been intensely pursued in the last years.[2,3] A significant part of the research efforts from the wet chemistry trench have focused on the covalent attachment of molecular fragments to graphene. The addition of malonate-type carbanions and radicals, acylations, and a wide variety of cycloadditions, including [2 + 1], [2 + 2], [3 + 2], and [4 + 2], have all been explored, among others.[4−7] Negative consequences of graphene's planar geometry are its insolubility and its tendency to reaggregate to form graphite through $\pi−\pi$ and van der Waals interactions. Such issues can be solved using graphene on a suitable substrate (for a recent review see Criado et al.[8]). It has been demonstrated that graphene grown or deposited on a substrate can physisorb or chemisorb molecules. Weakly attached adsorbates can act as donors or acceptors leading to changes in carrier concentration that allow the detection of single molecules[9] or the formation of intermolecular bands with long-range magnetic order at low temperatures.[10] Beyond the supramolecular functionalization of epitaxial graphene, its covalent modification has been proposed as an ideal tool for adjusting the electronic, optical, or magnetic properties. The chemical oxidation of graphene in ultrahigh vacuum (UHV)

conditions has also been demonstrated.[11,12] The attachment of hydrogen to each atomic site of the graphene lattice to create graphane was proposed,[13] resulting in a change in the hybridization of carbon atoms from sp^2 to sp^3, as well as the opening of a sizable gap at the Dirac point.[14−16] In these experiments, all of the atoms in the graphene lattice exhibit very similar reactivity, and the only way to get an atomically well-defined long-range order is to saturate all the atomic sites, creating a completely new material, e.g., graphane or graphene oxide. This lack of selectivity is a major drawback if the objective of the covalent modification is to modulate the electronic properties of graphene. It has been predicted that a periodic patterning of graphene would lead to new electronic properties[17] including a direct relation between the periodicity and the bandgap amplitude.[18,19] Therefore, the chemical functionalization of graphene in a periodic fashion with a periodicity in the range of 1−5 nm is highly desirable.

There have been several approaches for obtaining site selectivity in the chemical functionalization of graphene. One approach relies on patterning the surface using an atomic force microscope (AFM).[20,21] The main drawback of this approach is the time needed to write the motifs and also the difficulty of scaling up the process to millimeter size samples. Another

A
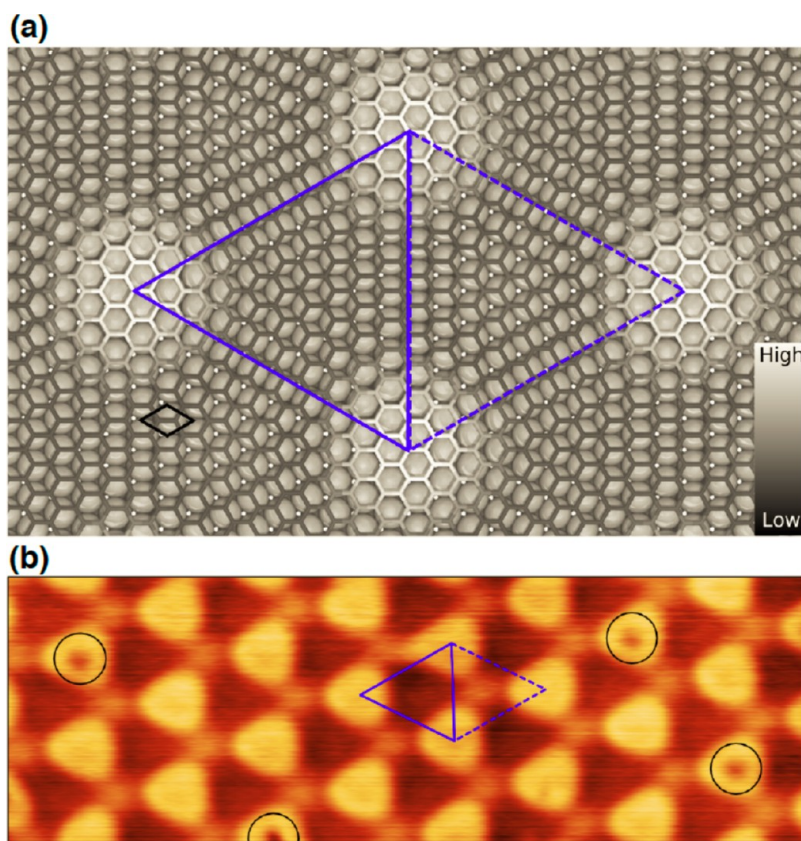
Figure 1. (a) Model of the gr/Ru(0001) surface, where gray circles represent the Ru atoms of the first atomic layer. The graphene hexagonal lattice is shown in a black to white color scale to indicate the height of the carbon atoms respect to the Ru(0001) surface. The unit cell of the moiré pattern is highlighted by two blue triangles. At the vertices all carbon atoms fall on 3-fold hollow sites of the Ru(0001) surface. At the center of the solid (dashed) triangle one carbon sublattice falls on FCC-stacked (HCP-stacked) 3-fold hollow sites and the other one on top positions. These two regions are named "FCC-Top" and "HCP-Top" respectively. (b) STM image acquired on pristine gr/Ru(0001) (24×7 nm^2; V_b = +1.5 V, I_t = 30 pA). The moiré pattern arising from the lattice mismatch is highlighted in blue. The HCP-Top area is marked with the dashed triangle, and the FCC-Top area is marked the solid triangle. Four point defects on the atop areas are indicated by black circles.

approach relies on the fact that strain and curvature strongly enhance the local reactivity of graphene,[22,23] although so far no long-range order has been achieved. Graphene grown on metallic substrates presents a moiré pattern due to the difference in lattice parameter between graphene and the substrate.[24] In particular, graphene grown on Ir(111) has been used to study the influence of a spatially ordered covalent functionalization in the graphene electronic structure.[25,26] Due to the weak interaction between the graphene and the Ir(111) substrate, the moiré pattern presents several rotational domains with different periodicities.[27,28] The weak interaction with the substrate also renders all of the carbon atoms almost identical electronically, and no distinct reactive sites are present in the system. To the best of our knowledge, there have been no reports of covalent functionalization of graphene with atomic-level selectivity.

Here, we describe a method for the organic covalent modification of graphene with exquisite spatial periodicity at the atomic scale. We take advantage of the fact that the growth of graphene on lattice-mismatched metallic substrates allows us to tailor the geometric and electronic properties of the graphene overlayer in a periodic fashion. In particular, we use graphene grown on Ru(0001) that presents a moiré pattern with a periodicity of ≈3 nm. The moiré shows periodically distributed areas where the charge transfer due to the interaction between graphene and ruthenium is rather large

and, as a consequence, these graphene areas present higher chemical reactivity. This point is illustrated by demonstrating that cyanomethyl radicals (CH$_2$CN$^\bullet$) produced by homolytic breaking of acetonitrile (CH$_3$CN) in UHV by electron bombardment bind to graphene preferentially at specific atomic sites with a nearly complete selectivity (>98%).

Growth of graphene through chemical vapor deposition (CVD) on a variety of metallic substrates is one of the preferred methods for the synthesis of high-quality graphene.[29−32] This method presents the additional advantage that the strength of the interaction between graphene and the metallic substrate can be tuned by varying the chemical nature of the latter.[33] In this respect, some of us have previously reported the epitaxial growth of graphene on Ru(0001) (hereafter, gr/Ru(0001)) where due to the mismatch between the hexagonal lattices of graphene and Ru, the system presents a moiré pattern with a surface periodicity of 2.93 nm[34] (see Supporting Information A for further details). Figure 1a shows that three different areas can be distinguished inside the moiré unit cell depending on the registry between the carbon atoms and the last two ruthenium atomic layers, namely, the "atop" region where all carbon atoms are placed above 3-fold hollow sites of the Ru surface (vertex of the blue triangles in Figure 1a), the "HCP-Top" region where half of the carbon atoms are located on HCP 3-fold positions and the other half on top of Ru atoms (dashed blue triangle in Figure 1a) and the "FCC-
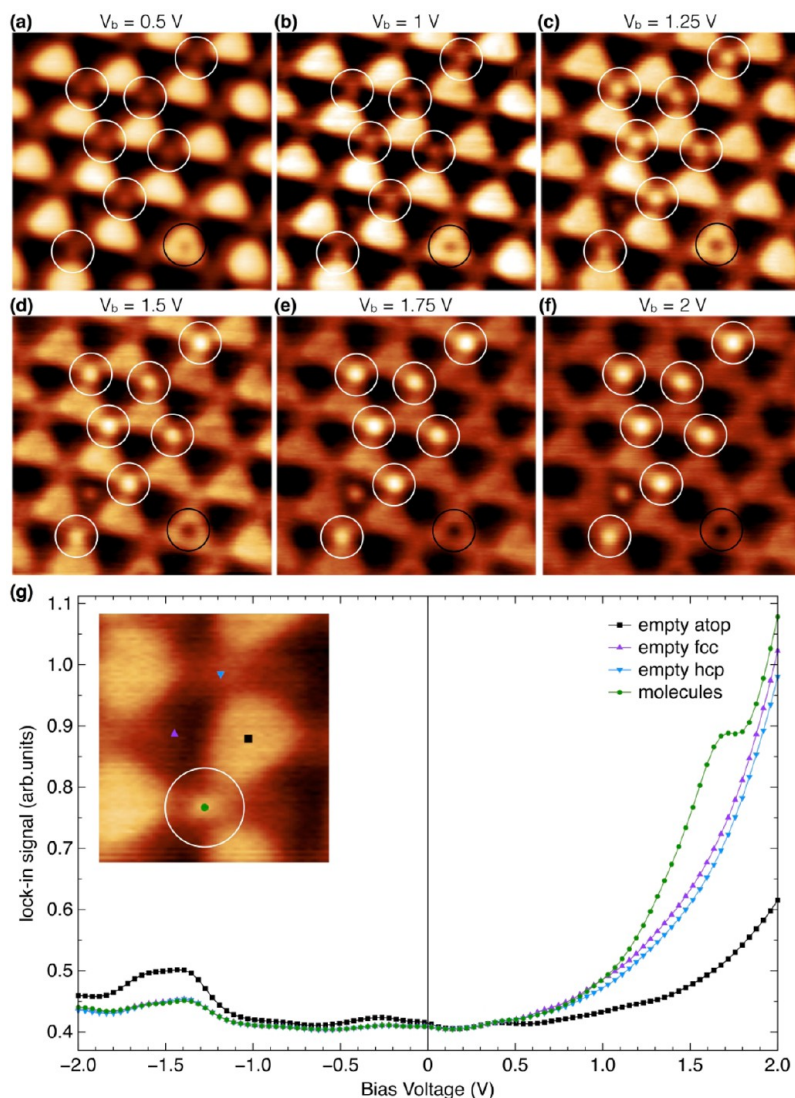
Figure 2. (a−f) $10 \times 10 \ nm^2$ STM images with different bias voltages acquired at 80 K after exposing gr/Ru(0001) to 180 Langmuir of acetonitrile at 300 K. Notice the related presence of seven bright bumps on HCP-Top sites (marked with a white circle), one on FCC-Top site and one graphene point defect (marked with a black circle). (g) Differential conductance, dI/dV, curves recorded at 80 K with the tip of the STM placed on top of the molecular attachments (green), the FCC-Top, HCP-Top (purple and blue, respectively), and the ripples (black) areas of the moiré pattern of gr/Ru(0001). The dI/dV individual curves were measured in open feedback loop conditions with the tunneling gap stabilized at +0.3 V and 50 pA. The lock-in signal was acquired using a modulation in the bias voltage of 40 mV (rms), a frequency of 856 Hz, and a time constant of 10 ms.

Top" region where half of the carbon atoms are located on FCC 3-fold positions and the other half on top of Ru atoms (solid blue triangle in Figure 1a).

Figure 1b shows a scanning tunneling microscope (STM) topographic image of the surface measured at +1.5 V bias voltage. Under these bias conditions, the moiré appears as a hexagonal array of bumps with a small corrugation (∼40 pm). The origin of the bumps is the change in registry within the moiré unit cell that produces a spatial modulation in the interaction between the C and Ru atoms, from weak van der Waals interaction in the high areas of the STM images to strong interaction in the lower areas.[35,36] This spatial variation of the interaction modulates all surface electronic properties, from the surface potential[37] to the electronic structure around the Fermi level,[34] which directly affects the chemical reactivity. The STM imaging conditions of Figure 1b also reveal the presence of four point defects on top of the ripples (marked with black circles),

which we attribute to subsurface oxygen trapped during the graphene growth process (see Supporting Information B for details).

Recently, Ruoff, Bielawsky, and co-workers have introduced a method for the selective functionalization of graphene on areas with high local curvature.[22] Considering this, and the seminal work by Balog et al. on the patterned hydrogenation of graphene on Ir,[25] we reasoned that graphene on Ru(0001) seems an ideal playground to exploit a similar strategy for a *periodic* chemical modification of graphene with subnanoscale selectivity. The metal−graphene interaction in gr/Ru(0001) is sufficiently strong to affect the chemical reactivity of specific atomic sites of the graphene overlayer, due to the presence of the moiré-related corrugation. While attempting to reproduce the wet-chemistry reaction conditions, we serendipitously discovered that gr/Ru(0001) can be functionalized by cyanomethyl radicals with exquisite spatial selectivity (see

C
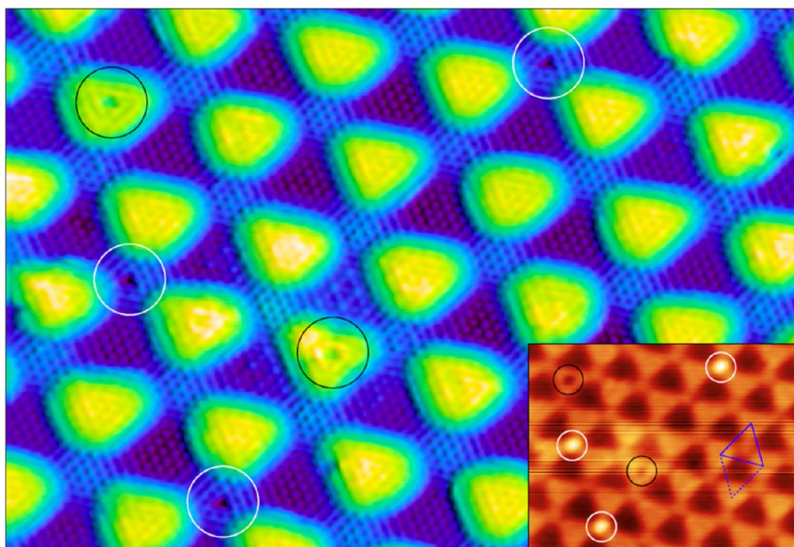
Figure 3. High resolution STM image (17×12 nm^2, V_b = 2 mV, I_t = 800 pA), acquired at 80 K on a region containing three molecular attachments (white circles) and two oxygen-related defects on graphene (black circles). Inset: Same region scanned afterward with V_b = +1.7 V and I_t = 100 pA. All three molecular attachments are still in place. The moiré unit cell is highlighted in blue in the inset.

Supporting Information C for details). Representative STM images are shown in Figure 2a−f, measured at 80 K as a function of the sample bias voltage after exposure of the sample at room temperature to 1×10^{-6} Torr of CH$_3$CN for 3 min, equivalent to 180 Langmuirs. Bright bumps related to the adsorption of acetonitrile, located exclusively at the valleys and the HCP-top sites, are observed for voltages between +1.25 V and +2 V. The molecular attachments show an apparent height of 26 ± 2 pm and a lateral width of 560 ± 20 pm at +1.5 V. The shape and size of the molecular attachments are very similar to those measured on STM images taken of acetonitrile adsorbed on Pt(111).[38] Figure 2g shows scanning tunnelling spectroscopy (STS) recorded on various positions of the moiré unit cell. The curves measured on top of the ripples, and the ones measured on the (empty) low areas of the moiré show the well-known asymmetry between the occupied and empty density of states of gr/Ru(0001).[34] The curves measured on the molecular attachments present an additional peak at +1.6 eV identified as the lowest unoccupied molecular orbital (LUMO). The energy of the highest occupied molecular orbital (HOMO) is below −2.0 V and, therefore, out of the measured energy window. The images confirm that for bias voltages below +0.5 V the molecular attachments are not visible, since tunneling is being carried out in the gap between the HOMO and LUMO. For bias voltages larger than +2.5 V the reduction in the apparent corrugation of the moiré pattern and its subsequent inversion[39] hinders the precise identification of the adsorption site of the molecular attachments.

Remarkably, single molecular attachments can be observed exclusively at the valleys of the moiré pattern. Moreover, there is a strong preference for HCP-Top sites over FCC-top regions offering another level of selectivity. For higher coverages on the order of 0.50 acetonitrile molecules per moiré unit cell, $98 \pm 1\%$ of the HCP-Top and $2 \pm 1\%$ of the FCC-Top areas of the unit cells are occupied. The same site preference has been observed for TCNQ[40] and F$_4$-TCNQ[41] molecules adsorbed on gr/Ru(0001) and can be understood considering the difference in the electronic structure between the FCC-Top and HCP-Top areas.[40]

In the present case, however, the bonding between the adsorbed molecular attachments and graphene relies on a strong C−C covalent bond, which modifies the sp^2 hybridization of a single C atom in graphene. This is demonstrated in Figure 3, in which a region containing three molecular attachments located in HCP-Top regions, encircled in white, is imaged with atomic resolution. The STM image has been taken in conditions where the molecular attachment is transparent (2 mV bias and 800 pA current) because the small bias voltage is probing the energy gap between HOMO and LUMO of the adsorbed molecule. Accordingly, the tip does not move up when it is located on top of the molecules attached to the surface. Simultaneously, the C atoms with a modified hybridization where the three molecules are bonded appear as single atom "holes" (see Supporting Information F3 and Figure S7 for details). Remarkably, the covalent attachments are located exclusively on crystallographically identical carbon atoms of the graphene overlayer. The inset shows the bright bumps of the molecules adsorbed on the "hole" sites by restoring a bias voltage where they can be imaged through their LUMO orbitals. In spite of the harsh imaging conditions all three molecules remain in place, without any noticeable change in shape or position. Going down to atomic resolution parameters without sweeping the molecular attachments away during the scan is contrary to what happens with physisorbed or even strongly chemisorbed isolated molecules, such as TCNQ[9] or F$_4$-TCNQ,[42] indicating the covalent nature of their attachment to graphene. In fact, the molecular attachments cannot be displaced from their adsorption sites by the STM tip following standard manipulation techniques.[43,44] Annealing the sample in UHV further confirms the strong bond between graphene and the molecular attachments. The sample remains unaltered up to 573 K.

These facts confirm the selective covalent patterning of gr/Ru(0001) through treatment with CH$_3$CN beyond reasonable doubt. Given the relatively inert nature of CH$_3$CN, and knowing that under high-vacuum (10^{-6} Torr) conditions ion gauges produce and emit active chemical species through ionization of the residual gases in the vacuum chamber, which can be adsorbed onto graphene,[45] we reasoned the same

process may take place during the exposure of the graphene surface to the acetonitrile molecules in UHV, since we use an ion gauge to measure the partial pressure of the acetonitrile gas. In order to gather experimental evidence of the molecular fragments that can be produced in the ion gauge during the CH_3CN exposition, we introduced in the UHV chamber the same partial pressure (1×10^{-6} Torr) of acetonitrile used during the graphene exposure and recorded the mass spectrum of the gas utilizing a quadrupole mass spectrometer (QMS) (see Supporting Information D for details). The ionization chamber of the QMS works under the same physical principle as the ion gauges and therefore the spectra measured is a reliable indicator of the chemical species produced in the ion gauge. The m/z pattern is perfectly consistent with a significant concentration of $CH_2CN^\bullet$ (Figure S3 and Supporting Information D for details). It is well-known that $CH_2CN^\bullet$ can be generated directly from CH_3CN by homolytic cleavage of a C−H bond.[46−48] Moreover, the cyanomethyl radical ($CH_2CN^\bullet$) is known to react with C−C double bonds[49−51] and arenes[52] forming C−C bonds.

To provide further experimental evidence for this hypothesis, we exposed the sample to 180 Langmuir of acetonitrile with the ion gauge in the preparation chamber turned *off*, and under these conditions *no* molecular attachments were detected on the surface (see Supporting Information G for further details).

To gain atomic understanding of the reaction, we ran DFT calculations for the adsorption of $CH_2CN^\bullet$ on gr/Ru(0001). The results are summarized in Figure 4. In agreement with the experimental data, the adsorption energies are within the limits of a covalent bond (>2.1 eV) (see Figure 4a). Remarkably, the HCP-Top/FCC-Top preference we observe experimentally is also reproduced. The two most stable configurations, HCP-Top(1) and HCP-Top(4), with adsorption energies of 2.34 and 2.49 eV are shown in Figure 4b and c. In this case, it is the alkyl carbon atom of $CH_2CN^\bullet$ that lies closer to the graphene surface, as is observed in the cycanomethylation of arenes.[52] The graphene carbon atom immediately below the CH_2CN addend is clearly displaced from the graphene mesh (see Supporting Information F for details). The shortest distance between an acetonitrile carbon atom and a graphene atom are 1.60 and 1.58 Å for the acetonitrile in the HCP-Top (1) and HCP-Top(4) adsorption geometries shown in Figure 4b and c, in very good accordance with a C−C single bond, for which the textbook C−C distance is 1.54 Å.[53] Other configurations considered and the corresponding adsorption energies are shown in Table S1 and Figure S6 and discussed in section F.3 of the SI. In contrast, identical calculations run with CH_3CN resulted in adsorption energies of 0.40 ± 0.03 eV and 0.42 ± 0.02 eV for the HCP-Top and FCC-Top regions, respectively, with the shortest acetonitrile−graphene distances >3 Å, indicative of physisorption, as expected (see Table S2 and Figure S8 in section F.3 of the SI).

To investigate the role of the Ru metallic substrate, we synthesized graphene on Ir(111) (hereafter, gr/Ir(111)), a system which exhibits a similar moiré pattern[54] but with almost negligible charge transfer and interaction between the carbon and iridium. Exposing gr/Ir(111) to 1×10^{-6} Torr of CH_3CN, no $CH_2CN^\bullet$ attachments were observed, confirming that the strong interaction between Ru and the graphene overlayer plays a fundamental role in the covalent functionalization (see Supporting Information E for details).

Due to the strong interaction between graphene and the Ru(0001) surface, the moiré pattern not only presents specific
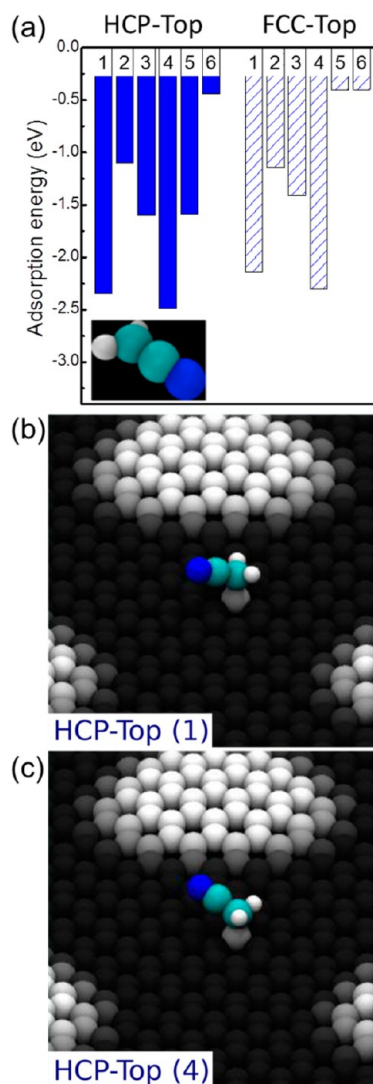
Figure 4. (a) Adsorption energies calculated for the different configurations of $CH_2CN^\bullet$ on the HCP-Top (solid boxes) and on the FCC-Top (empty boxes) regions of the gr/Ru(0001) moiré. The inset shows the ground state geometry of the corresponding molecule in the gas-phase. (b and c) Ground state adsorption geometries of the two most stable configurations of $CH_2CN^\bullet$ adsorbed in the HCP-Top region of the gr/Ru(0001) moiré. Graphene atoms are colored from dark-gray to white depending on their height. Carbon, nitrogen, and hydrogen atoms of the molecule are colored in cyan, blue, and white.

atomic sites with high chemical reactivity but long-range order as well. In this system, it is possible to grow graphene layers presenting lateral domain sizes exceeding 300 nm.[39,55] The large domain size together with the exquisite spatial selectivity of our functionalization method ensures the long-range order of the functionalized surface. Figure 5 shows a 66×40 nm^2 STM image of the functionalized gr/Ru(0001). In the image 50% of the moiré unit cells are occupied by one chemically bonded −CH$_2$CN molecule. Of those, 98.6% are bonded in the HCP-Top areas, while only 1.4% of the −CH$_2$CN are bonded to the FCC-TOP areas.

Similar results have been obtained for propionitrile, isobutyronitrile, and 2-phenylacetonitrile, demonstrating the applicability of this functionalization method to other molecular species (see Supporting Information H for details).
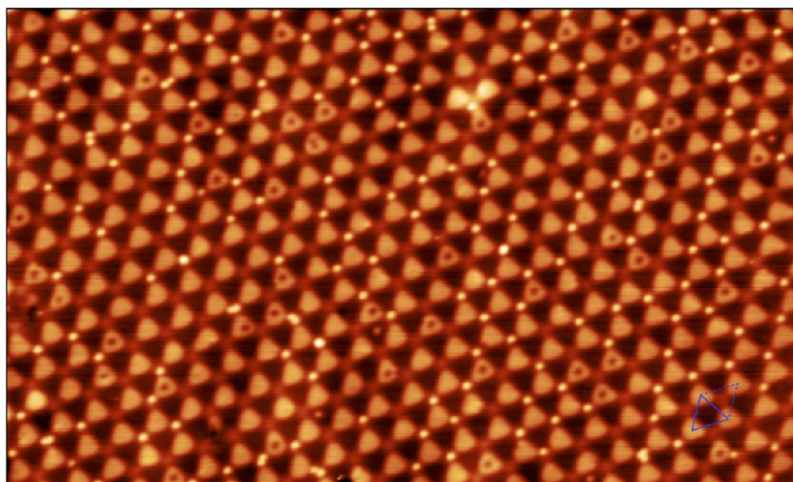
Figure 5. STM image (66×40 nm^2, $V_b = 1.7$ V, $I_t = 30$ pA) acquired at 80 K on a high coverage sample, prepared by exposing the gr/Ru(0001) surface to 600 Langmuir of acetonitrile at 300 K. The moiré unit cell is highlighted in blue.

In conclusion, we take advantage of the nanostructuration induced on graphene grown on Ru(0001) to chemically functionalize the graphene overlayer with atomic-level selectivity and exquisite spatial periodicity. The comparison between graphene grown on Ir(111) and graphene on Ru(0001) shows the importance of the interaction between the graphene and the metallic substrate that spatially modulates the properties of the graphene. Acetonitrile is homolytically broken by electron bombardment producing cyanomethyl radicals that react with the nanostructured graphene in a spatially modulated fashion. These results offer the possibility for tuning the graphene electronic, optic, or magnetic properties through an adequate covalent functionalization of single layer graphene with long-range order on the order of hundreds of nanometers and a periodicity of almost 3 nm. Moreover, identical results were obtained for propionitrile, isobutyronitrile, and 2-phenylacetonitrile, establishing a benchmark for the attachment of more complex molecular structures to specific atomic sites on graphene.

Methods. All experiments were performed in an UHV chamber with a base pressure of 5×10^{-11} Torr equipped with a low-temperature STM and facilities for tip and sample preparation. All of the STM measurements were carried out at 80 K. The graphene layer was prepared by keeping the Ru crystal at 1150 K in UHV while exposing it to an ethylene partial pressure of 8×10^{-8} Torr for 10 min. Acetonitrile was introduced in the UHV chamber via a leak valve to produce a partial pressure of 1×10^{-6} Torr. The values for the partial pressures of the different gases are measured using a Bayard-Alpert gauge calibrated for N$_2$. The details of the calculations are provided in the Supporting Information.

ASSOCIATED CONTENT

Ⓢ Supporting Information

The Supporting Information is available free of charge on the ACS Publications website at DOI: 10.1021/acs.nanolett.5b03928.

> Detailed discussion of the graphene/Ru(0001) structure. Oxygen contamination identification. Wet chemistry approach. Relative abundance of the cyanomethyl radical versus the acetonitrile molecule. Adsorption on graphene/Ir(111). Theoretical calculations. Ion gauge influence on the functionalization. Functionalization with different molecules (CH$_3$CH$_2$CN, (CH$_3$)$_2$CHCN, and Ph–CH$_2$CN) (PDF)

AUTHOR INFORMATION

Corresponding Authors
*E-mail: (A.L.V.d.P.) al.vazquezdeparga@uam.es.
*E-mail: (E.M.P.) emilio.perez@imdea.org.

Present Addresses
D.S.: Center for nanostructured Graphene, Department of Micro- and Nanotechnology, Technical University of Denmark, Ørsteds plads, Building 345B, DK-2800 Kgs., Lyngby, Denmark.
M.G.: Physik-Department E20, TU München, James-Franck str. 1, D-85748 Garching, Germany.

Author Contributions
The experiments and data analysis were carried out primarily by F.C. and J.J.N, with important contributions by A.B. R.B.-G. and M.G. S.L. performed the wet chemistry experiments. D.S. performed the theoretical calculations and contributed to the writing of the manuscript. D.G. contributed with the data analysis and contributed to the writing to the manuscript. R.M. contributed to the writing of the manuscript. E.M.P. and A.L.V.P. designed the experiments and wrote the manuscript with contributions from all authors.

Notes
The authors declare the following competing financial interest(s): The results here are partially protected under Spanish patent application P201530126.

REFERENCES

(1) Geim, A. K.; Novoselov, K. S. *Nat. Mater.* **2007**, *6*, 183−191.

(2) Georgakilas, V.; Otyepka, M.; Bourlinos, A. B.; Chandra, V.; Kim, N.; Kemp, K. C.; Hobza, P.; Zboril, R.; Kim, K. S. *Chem. Rev.* **2012**, *112*, 6156−6214.

(3) Chua, C. K.; Pumera, M. *Chem. Soc. Rev.* **2013**, *42*, 3222−3233.

(4) Park, J.; Yan, M. *Acc. Chem. Res.* **2013**, *46*, 181−189.

(5) Kuila, T.; Bose, S.; Mishra, A.; Khanra, P.; Kim, N. H.; Lee, J. H. *Prog. Mater. Sci.* **2012**, *57*, 1061−1105.

(6) Sun, Z.; James, D. K.; Tour, J. M. *J. Phys. Chem. Lett.* **2011**, *2*, 2425−2432.

(7) Criado, A.; Melchionna, M.; Marchesan, S.; Prato, M. *Angew. Chem., Int. Ed.* **2015**, *54*, 10734−10750.

(8) Criado, A.; Melchionna, M.; Marchesan, S.; Prato, M. *Angew. Chem., Int. Ed.* **2015**, *54*, 2−19.

(9) Schedin, F.; Geim, A. K.; Morozov, S. V.; Hill, E. W.; Blake, P.; Katsnelson, M. I.; Novoselov, K. S. *Nat. Mater.* **2007**, *6*, 652−655.

(10) Garnica, M.; Stradi, D.; Barja, S.; Calleja, F.; Díaz, C.; Alcamí, M.; Vázquez de Parga, A. L.; Martín, F.; Miranda, R. *Nat. Phys.* **2013**, *9*, 368−374.

(11) Vinogradov, N. A.; Schulte, K.; Ng, M. L.; Mikkelsen, A.; Lundgren, E.; Mårtensson, N.; Preobrajenski, A. B. *J. Phys. Chem. C* **2011**, *115*, 9568−9577.

(12) Hossain, M. Z.; Johns, J. E.; Bevan, K. H.; Karmel, H. J.; Liang, Y. T.; Yoshimoto, S.; Mukai, K.; Koitaya, T.; Yoshinobu, J.; Kawai, M.; Lear, A. M.; Kesmodel, L. L.; Tait, S. L.; Hersam, M. C. *Nat. Chem.* **2012**, *4*, 305−309.

(13) Sofo, J. O.; Chaudhari, A. S.; Barber, G. D. *Phys. Rev. B: Condens. Matter Mater. Phys.* **2007**, *75*, 153401.

(14) Boukhvalov, D. W.; Katsnelson, M. I.; Lichtenstein, A. I. *Phys. Rev. B: Condens. Matter Mater. Phys.* **2008**, *77*, 035427.

(15) Elias, D. C.; Nair, R. R.; Mohiuddin, T. M. G.; Morozov, S. V.; Blake, P.; Halsall, M. P.; Ferrari, A. C.; Boukhvalov, D. W.; Katsnelson, M. I.; Geim, A. K.; Novoselov, K. S. *Science* **2009**, *323*, 610−613.

(16) Haberer, D.; Vyalikh, D. V.; Taioli, S.; Dora, B.; Farjam, M.; Fink, J.; Marchenko, D.; Pichler, T.; Ziegler, K.; Simonucci, S.; Dresselhaus, M. S.; Knupfer, M.; Büchner, B.; Grüneis, A. *Nano Lett.* **2010**, *10*, 3360−3366.

(17) Park, C. H.; Yang, L.; Son, Y. W.; Cohen, M. L.; Louie, S. G. *Nat. Phys.* **2008**, *4*, 213−217.

(18) Ouyang, F.; Peng, S.; Liu, Z.; Liu, Z. *ACS Nano* **2011**, *5*, 4023−4030.

(19) Dvorak, M.; Oswald, W.; Wu, Z. *Sci. Rep.* **2013**, *3*, 2289.

(20) Bian, S.; Scott, A. M.; Cao, Y.; Liang, Y.; Osuna, S.; Houk, K. N.; Braunschweig, A. B. *J. Am. Chem. Soc.* **2013**, *135*, 9240−9243.

(21) Hossain, M. Z.; Walsh, M. A.; Hersam, M. C. *J. Am. Chem. Soc.* **2010**, *132*, 15399−15403.

(22) Wu, Q.; Wu, Y.; Hao, Y.; Geng, J.; Charlton, M.; Chen, S.; Ren, Y.; Ji, H.; Li, H.; Boukhvalov, D. W.; Piner, R. D.; Bielawski, C. W.; Ruoff, R. S. *Chem. Commun.* **2013**, *49*, 677−679.

(23) Bissett, M. A.; Konabe, S.; Okada, S.; Tsuji, M.; Ago, H. *ACS Nano* **2013**, *7*, 10335−10343.

(24) Vázquez de Parga, A. L.; Miranda, R. In *Graphene:Properties, preparation, characterisation and devices*; Chapter 6; Skakalova, V., Kaiser, A. B., Eds.; Woodhead Publishhing, 2014.

(25) Balog, R.; Jørgensen, B.; Nilsson, L.; Andersen, M.; Rienks, E.; Bianchi, M.; Fanetti, M.; Laegsgaard, E.; Baraldi, A.; Lizzit, S.; Sljivancanin, Z.; Besenbacher, F.; Hammer, B.; Pedersen, T. G.; Hofmann, P.; Hornekaer, L. *Nat. Mater.* **2010**, *9*, 315−319.

(26) Balog, R.; Andersen, M.; Jørgensen, B.; Slijvancanin, Z.; Hammer, B.; Baraldi, A.; Larciprete, R.; Hofmann, P.; Hornekaer, L.; Lizzit, S. *ACS Nano* **2013**, *7*, 3823−3832.

(27) Coraux, J.; N'Diaye, A. T.; Busse, C.; Michely, T. *Nano Lett.* **2008**, *8*, 565−570.

(28) Loginova, E.; Nie, S.; Thurmer, K.; Bartelt, N. C.; McCarty, K. F. *Phys. Rev. B: Condens. Matter Mater. Phys.* **2009**, *80*, 085430.

(29) Chae, S. J.; Günes, F.; Kim, K. K.; Kim, E. S.; Han, G. H.; Kim, S. M.; Shin, H. J.; Yoon, S. M.; Choi, J. Y.; Park, M. H.; Yang, C. W.; Pribat, D.; Lee, Y. H. *Adv. Mater.* **2009**, *21*, 2328−2333.

(30) Reina, A.; Jia, X.; Ho, J.; Nezich, D.; Son, H.; Bulovic, V.; Dresselhaus, M. S.; Kong, J. *Nano Lett.* **2009**, *9*, 30−35.

(31) Li, X.; Cai, X.; An, J.; Kim, S.; Nah, J.; Yang, D.; Piner, R.; Velamakanni, A.; Jung, I.; Tutuc, E.; Banerjee, S. K.; Colombo, L.; Ruoff, R. S. *Science* **2009**, *324*, 1312−1314.

(32) Lee, Y.; Bae, S.; Jang, H.; Jang, S.; Zhu, S. E.; Sim, S. H.; Song, Y. I.; Hong, B. H.; Ahn, J. H. *Nano Lett.* **2010**, *10*, 490−493.

(33) Preobrajenski, A. B.; Ng, M. L.; Vinogradov, A. S.; Martensson, N. *Phys. Rev. B: Condens. Matter Mater. Phys.* **2008**, *78*, 073401.

(34) Vazquez de Parga, A. L.; Calleja, F.; Borca, B.; Hinarejos, J. J.; Passeggi, M. G. C.; Guinea, F.; Miranda, R. *Phys. Rev. Lett.* **2008**, *100*, 056807.

(35) Stradi, D.; Barja, S.; Díaz, C.; Garnica, M.; Borca, B.; Hinarejos, J. J.; Sánchez-Portal, D.; Alcamí, M.; Arnau, A.; Vázquez de Parga, A. L.; Miranda, R.; Martín, F. *Phys. Rev. B: Condens. Matter Mater. Phys.* **2013**, *88*, 245401.

(36) Stradi, D.; Barja, S.; Díaz, C.; Garnica, M.; Borca, B.; Hinarejos, J. J.; Sánchez-Portal, D.; Alcamí, M.; Arnau, A.; Vázquez de Parga, A. L.; Miranda, R.; Martín, F. *Phys. Rev. Lett.* **2011**, *106*, 186102.

(37) Borca, B.; Barja, S.; Garnica, M.; Sánchez-Portal, D.; Silkin, V. M.; Chulkov, E. V.; Hermanns, C. F.; Hinarejos, J. J.; Vázquez de Parga, A. L.; Arnau, A.; Echenique, P. M.; Miranda, R. *Phys. Rev. Lett.* **2010**, *105*, 036804.

(38) Katano, S.; Kim, Y.; Trenary, M.; Kawai, M. *Chem. Commun.* **2013**, *49*, 4679−4681.

(39) Borca, B.; Barja, S.; Garnica, M.; Minniti, M.; Politano, A.; Rodríguez-García, J. M.; Hinarejos, J. J.; Farías, D.; Vázquez de Parga, A. L.; Miranda, R. *New J. Phys.* **2010**, *12*, 093018.

(40) Garnica, M.; Stradi, D.; Calleja, F.; Barja, S.; Díaz, C.; Alcamí, M.; Arnau, A.; Vázquez de Parga, A. L.; Martín, F.; Miranda, R. *Nano Lett.* **2014**, *14*, 4560−4567.

(41) Stradi, D.; Garnica, M.; Díaz, C.; Calleja, F.; Barja, S.; Alcamí, M.; Martín, N.; Arnau, A.; Vázquez de Parga, A. L.; Miranda, R.; Martín, F. *Nanoscale* **2014**, *6*, 15271−15279.

(42) Barja, S.; Garnica, M.; Hinarejos, J. J.; Vázquez de Parga, A. L.; Martín, N.; Miranda, R. *Chem. Commun.* **2009**, *46*, 8198−8200.

(43) Stroscio, J. A.; Eigler, D. M. *Science* **1991**, *254*, 1319−1326.

(44) Hla, S.-W. *J. Vac. Sci. Technol., B: Microelectron. Process. Phenom.* **2005**, *23*, 1351−1360.

(45) Caillier, C.; Ki, D. K.; Lisunova, Y.; Gaponenko, I.; Paruch, P.; Morpurgo, A. F. *Nanotechnology* **2013**, *24*, 405201.

(46) Lalevee, J.; Allonas, X.; Fouassier, J.-P. *J. Org. Chem.* **2005**, *70*, 814−819.

(47) Henry, D. J.; Parkinson, C. J.; Mayer, P. M.; Radom, L. *J. Phys. Chem. A* **2001**, *105*, 6750−6756.

(48) Coote, M. L. *J. Phys. Chem. A* **2004**, *108*, 3865−3872.

(49) Kukk, E.; Sankari, R.; Huttula, M.; Sankari, A.; Aksela, H.; Aksela, S. *J. Electron Spectrosc. Relat. Phenom.* **2007**, *155*, 141−147.

(50) Wu, J. Q.; Beranek, I.; Fischer, H. *Helv. Chim. Acta* **1995**, *78*, 194−214.

(51) Wong, M. W.; Radom, L. *J. Phys. Chem.* **1995**, *99*, 8582−8588.

(52) Yoshida, H.; Fujimura, Y.; Yuzawa, H.; Kumagai, J.; Yoshida, T. *Chem. Commun.* **2013**, *49*, 3793−3795.

(53) Cottrell, T. L. *The Strengths of Chemical Bonds*; Butterworth Scientific, 1978.

(54) N'Diaye, A. T.; Coraux, J.; Plasa, T. N.; Busse, C.; Michely, T. *New J. Phys.* **2008**, *10*, 043033.

(55) Sutter, P. W.; Flege, J. I.; Sutter, E. A. *Nat. Mater.* **2008**, *7*, 406−500.